

Lawrence Berkeley National Laboratory

Lawrence Berkeley National Laboratory

Title

Laboratory Investigations of a Low-Swirl Injector with H₂ and CH₄ at Gas Turbine Conditions

Permalink

<https://escholarship.org/uc/item/4gh8t82v>

Author

Cheng, R. K.

Publication Date

2009-10-12

Laboratory Investigations of a Low-swirl Injector with H₂ and CH₄ at Gas Turbine Conditions

R. K. Cheng and D. Littlejohn
*Environmental Energy Technologies Division
Lawrence Berkeley National Laboratory
Berkeley, CA 94720, USA*

P.A. Strakey and T. Sidwell
*National Energy Technology Laboratory
Morgantown, WV*

Abstract

Laboratory experiments were conducted at gas turbine and atmospheric conditions ($0.101 < P_0 < 0.810$ MPa, $298 < T_0 < 580$ K, $18 < U_0 < 60$ m/s) to characterize the overall behaviors and emissions of the turbulent premixed flames produced by a low-swirl injector (LSI) for gas turbines. The objective was to investigate the effects of hydrogen on the combustion processes for the adaptation to gas turbines in an IGCC power plant. The experiments at high pressures and temperatures showed that the LSI can operate with 100% H₂ at up to $\phi = 0.5$ and has a slightly higher flashback tolerance than an idealized high-swirl design. With increasing H₂ fuel concentration, the lifted LSI flame begins to shift closer to the exit and eventually attaches to the nozzle rim and assumes a different shape at 100% H₂. The STP experiments show the same phenomena. The analysis of velocity data from PIV shows that the stabilization mechanism of the LSI remains unchanged up to 60% H₂. The change in the flame position with increasing H₂ concentration is attributed to the increase in the turbulent flame speed. The NO_x emissions show a log linear dependency on the adiabatic flame temperature and the concentrations are similar to those obtained previously in a LSI prototype developed for natural gas. These results show that the LSI exhibits the same overall behaviors at STP and at gas turbine conditions. Such insight will be useful for scaling the LSI to operate at IGCC conditions.

NOMENCLATURE

a_x, a_r	normalized axial and radial stretch rates (1/mm)
α	reactants thermal diffusivity
c_{quench}	quenching factor $\alpha U_0/S_L^2 d$
d	injector diameter (mm)
K	S_T correlation parameter
$m = m_c/m_s$	ratio of the flows through the center-channel, m_c , and the swirl passage, m_s
M_r/M_0	recirculation strength: M_r mass flux of fluid with negative U , M_0 mass flux of the reactants
q'	2D turbulent kinetic energy = $_{-}(u'^2+v'^2)^{1/2}$
$R = R_c/R_i$	ratio of the center channel radius, R_c to injector radius, R_i
S	swirl number
S_L	laminar flame speed
S_T	turbulent flame speed
T_{ad}	adiabatic flame temperature
U_0	bulk flow velocity
x_f, x_x^*	leading edge and mean flame brush positions
x_o	virtual origin of divergent flow

1. INTRODUCTION

Integrated Gasification Combined Cycle (IGCC) is an advanced concept to reduce the emissions of greenhouse gases from coal power plants. Its basic premise is to extract syngas from coal that consists of primarily H_2 , CO and other diluents for burning in a gas turbine to generate electricity. When CO is separated from the syngas and converted to CO_2 for sequestration, the gas turbine operates on nearly 100% H_2 . This is the goal of the FutureGen Alliance which is a U.S. public-private partnership to develop near-zero emissions coal power plants. One of FutureGen's key components is a cost-competitive hydrogen turbine with ultra low NO_x emission and high efficiency. The goal of our research is to adapt our lean premixed low-swirl injector (LSI) [1-4] to the H_2 turbines.

For land-based power turbines, lean premixed combustion is a proven dry-low-NO_x (DLN) method to control NO_x < 10 ppm and CO < 15 ppm (both @ 15% O₂) without requiring exhaust gas cleanup. The use of hydrogen addition has been proposed as a means to extend the lean blow off limits to reach the ultra-low emission target of < 5 ppm NO_x [5]. Laboratory studies have shown that the addition of a modest amount of H₂ can change the global flame characteristics [6, 7]. Therefore, the combustor needs to be modified to operate effectively with hydrogen enriched fuels. Burning near 100% H₂ requires a substantial re-design of the combustor to address additional issues associated with the faster combustion chemistry of H₂ and its influences on processes such as flame anchoring, flame stability, flashback, and auto-ignition. Because of the high cost and risk involved in conducting H₂ experiment at gas turbine conditions and the propriety nature of the subject, there are very few basic studies on high pressure premixed turbulent H₂ flames in the scientific literature (e.g. [8]).

To start the development of LSI for H₂ we investigated diluted and undiluted H₂, CH₄ and CH₄/H₂ flames in open atmospheric condition [3, 9]. These flames showed that the H₂ influences on the flowfield and other flame features are less than those in a conventional high-swirl burner [6]. The purpose of this study is to extend the investigation to the operating conditions of typical gas turbines, i.e. $0.4 < P_0 < 2.0$ MPa, $450 < T_0 < 700$ K, $30 < U_0 < 80$ m/s, and to gain an overview of the functional changes in the global characteristics of the LSI flames with H₂ concentration, ϕ , P_0 , T_0 and U_0 . To assist in the interpretation of the high pressure results, velocity measurements by PIV were made for representative flames at STP.

2. BACKGROUND

The LSI [1, 3] is based on a flame stabilization concept developed for basic studies that has been adapted to industrial heaters [10-14]. Recent tests of a 7 MW gas turbines with a set of LSI show it to be a promising method to attain < 5 ppm NO_x for natural gas operation. The LSI has also been evaluated with fuels of a wide range of Wobbe indices and the results show it to be a fuel-flexible design [3].

The heart of the LSI is a swirler with an open center-channel that allows a portion of reactants to remain unswirled [15]. The nonswirling center flow inhibits vortex breakdown and promotes flow divergence that is the key aerodynamic feature for the low-swirl flame stabilization method. To control the mass ratio, m , between the un-swirled and swirled passages a perforated screen is placed at the entrance of the centerchannel (Fig. 1 bottom left). From Ref [1, 16] S is:

$$S = \frac{2}{3} \tan a \frac{1 - R^3}{1 - R^2 + m^2 \left(\frac{1}{R^2} - 1 \right)^2 R^2} \quad \text{Eq. 1}$$

Ref. [4] introduced an expression that explains why the LSI flame remains stationary regardless of U_0 . It stems from a velocity balanced at the leading edge of the flame brush, x_f .

$$1 - \frac{dU}{dx} \frac{(x_f - x_o)}{U_o} = \frac{S_T}{U_0} = \frac{S_L}{U_0} + \frac{Ku'}{U_o} \quad \text{Eq. 2}$$

On the LHS, $dU/dx/U_o$ is the normalized axial divergence rate a_x that has shown to be a constant because the nearfield of the LSI is self-similar. The far RHS is the normalized linear S_T correlation with an empirical constant, K based on previous measurements showing a non-bending linear S_T correlation for the detached flames low-swirl burners [17]. Of the two terms, the contribution from S_L/U_0 becomes small for large U_0 because S_L for ultra-lean flames

pertinent to gas turbines are typically < 1.0 m/s. The Ku'/U_0 term is dominant and is constant because u'/U_0 is controlled by the center-channel plate. Consequently, $x_f - x_0$ does not vary significantly for large U_0 .

A practical application of Eq. 2 is to predict the flashback velocity [4]. It also describes the fuel effects. Recent correlation of S_T shows that H_2 has a higher correlation constant K (3.17) than CH_4 (1.73^1) which implies an upstream shift in the H_2 flame position [9]. This simple model can be the basis for scaling the LSI to different sizes and conditions if the flame shift and turbulent flame speed correlation can be verified at gas turbine conditions.

3. EXPERIMENTAL SYSTEM AND DIAGNOSTICS

The high pressure experiments were performed in a facility called SimVal (Fig. 1) designed to provide data to support modeling and computational developments [5, 8]. SimVal consists of an optically-accessible idealized combustor capable of operating at T_0 up to 810 K and P_0 up to 2.31 MPa with maximum supplies of air at 1.23 kg/s, natural gas at 53.3 g/s and hydrogen at 2.3 g/s. The test section has four 10.2 cm wide by 30.5 cm windows with a central combustor liner that is a 31.8 cm long quartz tube of 18.0 cm I.D. This geometry is representative of a typical can-style combustor.

The LSI is similar to the one used previously [3]. It is sized to fit SimVal ($d = 5.715$ cm diameter) with $R = 0.66$. The number of vanes (16) and the swirl blade angle ($\alpha = 40^\circ$) are same as earlier versions and the swirler recess ($l_x = 4.6$ cm) is shorter. To meet the SimVal start-up requirement, a small (0.32 mm) pilot is embedded at the center of the perforated screen that is mounted in the upstream end of the center-channel. The pilot fuel was not used during the

experiments. This LSI has a swirl number of 0.5 similar to the one used in Ref [3]. The approach flow to the LSI is fully premixed and spatially uniform. The pressurized flames were monitored by a video camera capturing the visible luminosity (350 – 475 nm) from the CH₄ combustion emissions. The images were used to characterize flame shift and other changes in the global flame characteristics. A high speed (900 fps) OH chemiluminescence video camera was also used to capture the flashback events.

The STP experiments were performed in a separate combustor to facilitate the collection of a large data set for the flowfield analysis. It has the same inflow plenum, quartz liner and exit restriction as SimVal but without the outer liner and with an exit plate with a center opening instead of a cylindrical resonant exit section. Flowfield information was obtained by the PIV system described in Ref. [1, 3]. Data analysis was performed on 224 image pairs (13 by 13 cm field of view) using software developed by Wernet [18]. Due to deposition of the PIV seeds on the inner wall of the quartz tube, repeated runs were required at some conditions to collect the 224 image pairs. Flame shift and flame shape changes were investigated in a series of experiment by using the PIV camera to capture the visible luminosity of the CH₄ combustion.

The experimental conditions are summarized in Fig. 2. The pressurized preheated experiments were initiated by generating a NG flame (96.0% CH₄, 2.5% C₂H₆, 0.4% C₃H₈, and 0.7% N₂ and higher hydrocarbons) at a given temperature ($500 < T_0 < 600$ K), pressure ($0.101 < P_0 < .811$ MPa), velocity ($20 < U_0 < 60$) m/s, and equivalence ratio ($0.4 < \phi < 0.5$). After the flame reached a steady state and its emissions and flame position recorded, the H₂ concentration was gradually increased to 40%, then to 60%, 80%, and for some cases 100% while holding all other variables

¹ The correlation constant for hydrocarbon reported in Ref. [3] is deduced from data measured in all low-swirl burners. The 1.73 value is deduced from data from the LSI.

constant. Data from 46 flames were collected with the majority at $P_0 = 0.202, 0.405$ MPa and $U_0 = 40, 60$ m/s. These conditions are representative of the operation of a gas turbine at idling and partial load. The flashback limits for the high H_2 fuels were determined in separate runs in which ϕ was increased while holding the % H_2 , U_0 , T_0 , and P_0 constant until flashback occurred. Due to the hazards and safety risks of flashback tests, these experiments were not repeated. But by using a slow rate of increase in ϕ over 30 minutes the uncertainty at flashback was controlled to below 0.015. PIV measurements on six flames were conducted at $U_0 = 18$ m/s with $\phi = 0.59$ for CH_4 , $\phi = 0.48$ for 40% H_2 , and $\phi = 0.4$ for the 40, 60, 80, and 100% H_2 . The flow velocity at STP is at the low end of the high pressure experiments and the fuel and mixture conditions are compatible.

4. RESULTS

4.1. Global behavior of high pressure flames

The changes in the flame shape at high pressure and at STP with increasing H_2 fuel concentration are shown in Fig. 3. These images illustrate for the first time that the general features of LSI flames at gas turbine conditions are the same as those at STP. At 40% H_2 , both the STP and pressurized flames are lifted and have a bowl shape that is characteristic of the open LSI flames [3]. Increasing to 60% H_2 results in the flames shifting closer to the nozzle exit but the general shape remains unchanged. More significant changes are shown at $H_2 > 80\%$ where the flames are drawn to the exit and the flames attach to the rim of the LSI nozzle. This phenomenon also occurs in open H_2/CH_4 flames [9] where the high diffusivity of H_2 promotes burning in the outer shear layer and causes the flame to attach. At $H_2 > 92\%$, the STP and the high pressure flames become almost planar to suggest a change in the flame stabilization process.

Due to the high flame speeds of H₂ mixtures, addressing flashback is a major challenge for H₂ gas turbine. The ϕ_{FB} for the LSI determined at six conditions are listed in Table I. Though the results are limited, they show a trend of ϕ_{FB} increasing with U_0 and decreasing with H₂%. But the effect of pressure is still unclear. The changes in ϕ_{FB} with U_0 and % H₂ are consistent with the results obtained in SimVal from an idealized high-swirl configuration (SV-HSI) [19]. The values of ϕ_{FB} , however, indicate that the LSI has a slightly higher flashback resistance.

To characterize the difference in their flashback behavior, the quenching factor, C_{quench} , of Fritz et al. [20] was used. These authors show that the Peclet number at ϕ_{FB} $Pe_U = U_0 d / \alpha$ correlates with $Pe_{S_L} = S_L d / \alpha$ based on S_L . When reformulated in term of a quenching factor, $C_{quench} = \alpha U_0 / S_L^2 d$, C_{quench} is shown to be a function of the density ratio of unburnt to burnt gases ρ_u / ρ_b . Flashback resistance is associated with small values of C_{quench} that represents a short chemical time at flashback compared to the mean convective time. In Fig. 4, the C_{quench} values of LSI are generally lower than those from SV-HSI to show the LSI has a lesser propensity to flashback.

Fritz et al. attributed the physical process of flashback in a swirl burner to vortex bursting or baroclinic vorticity production by which a premixed flame can propagate through the core of a free vortex at speeds much higher than the laminar flame speed. This implies that vorticity production in the shear region of the flowfield is where flashback originates. This may explain the flashback resistance of the LSI because the shear stresses in its flowfield are less than that of a typical high-swirl burner [1].

4.2. Observations in STP flames and flowfield analysis

Six STP flames were selected to investigate how the changes in the global flame characteristics affect the flowfield and the stabilization mechanism. As shown in Fig. 3, increasing the H₂ fuel concentration pulled the STP flame closer to the dump plane. Flame attachment occurred at H₂ > 40% and the flame was fully attached at 60%. The 80% H₂ flame exhibited fluctuating behavior due to intermittent burning in the outer recirculation zone that changed the flame brush from “M” shape to a planar shape. The 100% H₂ flame was compact in appearance and produced high-frequency audible broad-band flame noise that was louder than the quieter lower frequency broad band noises produced by the CH₄/H₂ flames. The change in the sound signature was not associated with chamber acoustic because it was also found in the open flames. This phenomenon may be indicative of the differences in the fundamental processes of H₂ and hydrocarbon flames.

The influence of the outer recirculation zone on the high H₂ flames was also reported in the high-swirl burner studies of Schefer et al. [6] and Strakey et al. [5]. Schefer et al. observed burning in the outer recirculation zone at relatively low H₂ concentration of 29% and Strakey et al. found flame anchoring in the outer recirculation prior to lean blow-off. Therefore, the outer recirculation zone is a significant controlling process of the H₂ flames in a swirling combustion system.

The mean velocity vectors for three flames are compared in Fig. 5. These PIV data are contaminated by laser reflections from the quartz enclosure and by particle deposition on the inner wall. However, the affected regions are away from the centerline and the nearfield ($x/D < 0.5$) where the analyses are performed. In Fig. 5(a), the nearfield features of the detached 40% H₂ flame such as the central divergent zone are the same as those reported previously for open H₂/CH₄ flames [3]. The main difference is the formation of the outer recirculation zone shown by

the inward velocity vectors at the lower side boundaries. In the farfield, a broad central recirculation zone is shown. As reported in Ref. [21], the strength of the central recirculation ($M_r/M_0 = 0.06$ at $x/D = 2$) is affected by the enclosure size and the heat release rate, but it has no influence on the flame brush upstream. In Fig 5(b) the overall flowfield of the 60% H₂ flame remain unchanged. Therefore, burning in the shear layer and flame attachment do not seem to have a significant influence on the mean flowfield. In the farfield, reductions in the size and strength of the central recirculation zone are found ($M_r/M_0 = 0.02$ at $x/D = 2$). More significant changes are found in the flowfield of the 80% H₂ flame of Fig. 5(c). As discussed above, this flame was fully attached and the planar-shaped flame occupied most of the nearfield. Therefore, the PIV domain captured mostly the flow within the products region.

The centerline velocity profiles in Fig. 6 illustrate the similarity and differences of the six STP flames. In Fig. 6(a), the nearfield regions of the 0 % to 60% H₂ flames are consistent and show divergent regions with linear U/U_0 decays. These profiles deviate at $x > 30$ mm due to differences in the heat releases. The U/U_0 profiles of the two flames with H₂ \geq 80% have different features with lower nearfield decay rates and higher flow acceleration in the farfield. The q'/U_0 profiles in Fig. 6 (b) show relatively flat regions up to $x = 50$ mm. The increases in the scatter of the q'/U_0 data in the farfield for the three flames with H₂ $>$ 60% are symptoms of data degradation because the particle deposition problem was exacerbated by burning in the outer recirculation zone. The relatively flat q'/U_0 distributions shown by the three other flames are consistent with those observed in open flames.

As discussed previously [3, 4, 9], the centerline velocity profiles are used to deduce the four parameters in Eq. 2 that characterize the nearfield region. The virtual origin, x_0 , and the normalized axial stretch rate, $a_x = (dU/dx)/U_0$ are deduced by linear fit and extrapolation of the

U/U_0 profile in the nearfield divergent regions at $x < 30$ mm. The turbulent flame speed S_T , is defined as the axial velocity at the leading edge flame positions, x_f according to the procedure described in Ref [4]. The x_0 , a_x and S_T results are shown in Fig. 7. The x_f results will be presented later. In Fig 7 (a) and (b), x_0 and a_x remain unchanged up to $H_2 = 60\%$. Their values of $x_0 = -15$ mm are slightly larger than those reported in Ref [3, 4, 9] because this LSI generated more lifted flames. The mean a_x value of -0.18 mm^{-1} , however, is typical of those reported for open and enclosed flames burning pure or blended hydrocarbon and H_2 fuels. The abrupt changes in x_0 and a_x at 80% H_2 are clearly the consequences of flame attachment.

The S_T for the flames with $H_2 \leq 60\%$ are compared in Fig 7 (c) with those measured in the LSI for CH_4 , H_2 and various fuel blends. This plot differs from previous version (e.g. [3, 4, 9]) in two ways. First, the normalization uses S_L data for CH_4 by Jomaas et. al [22] and S_L for H_2 and fuel blends computed by CHEMKIN-PREMIX using GRI 3.0. Second, only the S_T data from the LSI are shown. The use of updated S_L and a specific data set does not change the main conclusion that the S_T from LSI correlates linearly with u' and that H_2 has a higher S_T correlation constant K than CH_4 . The implication is that the S_T of the blended fuels should fall within the region bounded by the two linear correlations. The four data points from this study support this notion despite the fact that these are enclosed flames and have some of the largest values of S_T/S_L and u'/S_L .

Figure 8 shows radial profiles at $x = 15$ mm for the STP flames. The U/U_0 profiles in Fig 8(a) all collapse on to a consistent distribution that has a relatively flat region at the center flanked by two asymmetric peaks corresponding to the swirl annulus shear regions. Closer examination shows slight outward expansion of the shear regions with increasing $H_2\%$ due to burning in the outer recirculation zones. In Fig 8(b), the v/U_0 profiles for the four flames with $H_2 < 80\%$ show a

linear central region with a_r of -0.009 mm^{-1} . Therefore, these enclosed flames also exhibit a 2:1 ratio between a_x and a_r as in the open flames. At $H_2 > 80\%$, a_r reduces slightly to -0.005 mm^{-1} and is accompanied by higher radial outflow in the shear regions indicated by the larger minimum and maximum peaks. In Fig 8(c), the q'/U_0 levels in the center region for all flames are consistent. But in the swirling shear region, significant increases in the turbulence levels are shown by the $H_2 = 80\%$ and pure H_2 flames. Again, this is a consequence of burning in the shear region.

The PIV results confirm that the nearfield self-similarity flow features are preserved up to 60% H_2 despite the fact that the flame begins to attach to the rim at $H_2 > 40\%$. Therefore, flame propagation in the divergent central regions remains the dominant process. With $H_2 \geq 80\%$, burning in the outer recirculation and within the shear regions become dominant. In addition to altering the flowfield, the increase in turbulence level within the shear region may provide a flashback pathway.

4.3. Flame shift and NO_x emissions

To quantify flame shift, x_f^* were deduced from the flame luminosity images by the steepest gradient points on the centerline intensity profiles. In the absence of laser-based data at elevated T_0 and P_0 , x_f^* is a sufficiently well-defined parameter to characterize flame position because it relates directly to x_f . The set of high pressure flame data was analyzed to examine their sensitivity to T_0 , P_0 , U_0 and % H_2 . The result (Fig. 9) shows that x_f^* for the pressurized flames is the same at x_f for the STP flames. Both x_f^* and x_f are sensitive to % H_2 . Changing U_0 , as illustrated by the three inserts does not have a strong effect on x_f^* . This shows that Eq. (2) describing the coupling between the divergent flowfield and turbulent flame speed should also apply to gas turbine conditions.

Eq. (2) also shows that the flame shift due to H₂ is associated with the higher value of K . To determine if this model is qualitatively correct, x_f for a lean CH₄ and a lean H₂ flame were computed using $x_0 = -15$ mm, $a_x = -0.018$, $u'/U_0 = 0.1$, and $U_0 = 20$ m/s. A heavy broken line joining the two points is shown in Fig 9 with the underlying assumption that K is a monotonically increasing function with % H₂. The slope of the model prediction is in general agreement with x_f^* but is less than that of the STP flames on which the two values of K were based. The difference is due to flame attachment at high % H₂ drawing the flame closer to the nozzle and changing the x_0 and a_x .

The NO_x emissions are shown Fig 10 and they are compared with the correlation from Leonard and Stegmaier [23] that is considered by the gas turbine community to be the reference for a well-designed premixed combustion system. Also shown are logarithmic fits of the emissions from natural gas LSI [1] and SV-HSI [8]. For the mixtures with up to 60% H₂ the NO_x emissions from the LSI are close to the reference Leonard and Stegmaier correlation and to those reported previously. This supports the conclusion of Leonard and Stegmaier that the NO_x emission from a well-designed natural-gas premixed combustion system is predominantly a function T_{ad} at $T_{ad} < 1900$ K. There is however a slight increasing trend with $H_2 \geq 80\%$ that is especially noticeable at $T_{ad} < 1750$ K. A similar trend has also been observed in SV-HSI. As these NO_x data are among the first to be reported for premixed H₂ flames at gas turbine conditions, much more needs to be done to determine the cause of this upward shift.

5. DISCUSSION

Our studies show that the basic LSI design is amenable to burning pure H₂ at gas turbine conditions. The flame shapes and the flame shifts at STP and gas turbine conditions are the same.

The main implication is that except for fuels with very high % H₂ the physical processes at high T₀ and P₀ can be explained by a simple model that describes the coupling between the self-similar nearfield flow divergence and linear turbulent flame speed correlation. This provides a foundation for future studies to verify this model at gas turbine conditions so that it can be used for scaling the LSI design to different sizes, fuels, and operating conditions. From an experimental perspective, the knowledge that the STP experiments provide relevant and useful information can reduce the reliance on costly and time-consuming high pressure runs.

Another significant observation is that the change in flame shape at high H₂% is strongly affected by burning in the outer recirculation zone. The process pulled the flame close to the LSI exit where turbulence intensities are higher. Although it is difficult to quantify, close examination of the flashback high speed videos shows that flashback does not originate at the nozzle wall but in the region of high q'/U_0 in Fig. 8(c). Therefore, changing the dump-plane geometry to eliminate the outer recirculation may improve the LSI flashback resistance and perhaps NO_x performance for high H₂ fuels.

6. CONCLUSIONS

Laboratory experiments have been performed to investigate the operation of a low-swirl injector with natural gas and H₂ at atmospheric and gas turbine conditions of $500 < T_0 < 600$ K, $0.101 < P_0 < .811$ MPa, and $20 < U_0 < 60$ m/s. The flashback limits show that the LSI has a slightly higher flashback resistance than an idealized high-swirl design. The primary effect of H₂ is to draw the flame closer to the dump plane. At H₂ > 80% the flame attaches to the rim and changes into disk shape due to burning in the outer recirculation zone. The STP flames exhibit similar behavior and analysis of their flowfields and turbulent flame speed showed that the flame

stabilization mechanism remains unchanged up to 60% H₂. An analytical model shows that upstream shift in the flame position with increasing H₂ concentration is associated with the higher S_T correlation constant for H₂. The trend predicted by this model is consistent with the trends observed at gas turbine conditions. This implies that nearfield flow-similarity and linear S_T correlation are relevant at gas turbine conditions. Further experimental studies are needed to verify this coupling. NO_x emissions show log linear dependence on T_{ad} and are consistent with those of a well-designed premixed combustion system. A slight upward shift in NO_x for high H₂ flame is also observed and requires further study to identify the mechanism for the excess NO_x production.

This study verified earlier conjecture that the LSI does not need to undergo significant alterations to operate with H₂. But the LSI design for H₂ turbines needs to address the influence due to burning in the outer recirculation zone.

7. ACKNOWLEDGEMENT

Support of this work was provided by US Dept. of Fossil Energy under Contract No. DE-AC03-76F00098. The support of the U.S. DOE Turbines program is also gratefully acknowledged for the testing performed at NETL

8. REFERENCES

- [1] M. R. Johnson, D. Littlejohn, W. A. Nazeer, K. O. Smith and R. K. Cheng, Proc. Comb. Inst, 30 ((2005) 2867 - 2874.
- [2] W. A. Nazeer, K. O. Smith, P. Sheppard, R. K. Cheng and D. Littlejohn, ASME Turbo Expo 2006: Power for Land, Sea and Air, ASME, Barcelona, Spain, 2006, ASME GT2006-90150
- [3] D. Littlejohn and R. K. Cheng, Proc. Comb. Inst., 31 (2) (2007) 3155-3162.

- [4] R. K. Cheng, D. Littlejohn, W. A. Nazeer and K. O. Smith, *Journal of Engineering for Gas Turbines and Power*, 130 (2) (2008) 21501-21511.
- [5] P. Strakey, T. Sidwell and J. Ontko, *Proceedings of the Combustion Institute*, 31 (2) (2007) 3173-3180.
- [6] R. W. Schefer, D. M. Wicksall and A. K. Agrawal, *Proc. Comb. Inst.*, 29 ((2002) 843-851.
- [7] O. Tuncer, S. Acharya and J.-H. Uhm, *ASME Turbo Expo*, Montreal, Canada, 2007, GT2007-28158.
- [8] T. Sidwell, G. Richards, K. Casleton, D. Straub, D. Maloney, P. Strakey, D. Ferguson, S. Beer and S. Woodruff, *Aiaa Journal*, 44 (3) (2006) 434-443.
- [9] R. K. Cheng and D. Littlejohn, *Journal of Engineering for Gas Turbines and Power*, 130 ((2008) 31503-31511.
- [10] C. K. Chan, K. S. Lau, W. K. Chin and R. K. Cheng, *Proc. Comb. Inst.*, 24 ((1992) 511-518.
- [11] R. K. Cheng, D. A. Schmidt, L. Arellano and K. O. Smith, *IJPGC2001*, New Orleans, 2001,
- [12] I. G. Shepherd, R. K. Cheng, T. Plessing, C. Kortschik and N. Peters, *Proc. Comb. Institute*, (29) (2002) 1833 - 1840.
- [13] C. Kortschik, T. Plessing and N. Peters, *Combustion and Flame*, 136 (1-2) (2004) 43-50.
- [14] P. Petersson, J. Olofsson, C. Brackman, H. Seyfried, J. Zetterberg, M. Richter, M. Alden, M. A. Linne, R. K. Cheng, A. Nauert, D. Geyer and A. Dreizler, *Applied Optics*, 46 (19) (2007) 3928-3936.
- [15] R. K. Cheng, D. T. Yegian, M. M. Miyasato, G. S. Samuelsen, R. Pellizzari, P. Loftus and C. Benson, *Proc. Comb. Inst.*, 28 ((2000) 1305-1313.
- [16] D. Littlejohn, M. J. Majeski, S. Tonse, C. Castaldini and R. K. Cheng, *Proc. Comb. Inst.*, 29 ((2002) 1115 - 1121.
- [17] B. Bedat and R. K. Cheng, *Combustion and Flame*, 100 (3) (1995) 485-494.
- [18] M. P. Wernet, *18th International Congress on Instrumentation for Aerospace Simulation Facilities*, Toulouse, France, 1999,
- [19] G. Eggenpieler, P. A. Stakey and T. Sidwell, *46th AIAA Space Sciences Meeting*, Reno, NV, 2008,

- [20] J. Fritz, M. Kroner and T. Sattelmayer, *Journal of Engineering for Gas Turbines and Power-Transactions of the Asme*, 126 (2) (2004) 276-283.
- [21] R. K. Cheng and D. Littlejohn, *Turbo Expo 2008*, ASME, Berlin, Germany, 2008,
- [22] G. Jomaas, X. L. Zheng, D. L. Zhu and C. K. Law, *Proceedings of the Combustion Institute*, 30 (1) (2005) 193-200.
- [23] G. Leonard and J. Stegmaier, *Journal of Engineering for Gas Turbines and Power-Transactions of the Asme*, 116 (3) (1994) 542-546.

Table I Conditions at flashback

H ₂ %	P ₀ Mpa	T ₀ K	U ₀ m/s	ϕ _{FB}
100	0.202	530	20	0.5
100	0.202	550	30	0.57
87	0.405	560	20	0.52
100	0.405	570	30	0.4
82	0.810	575	20	0.49
92	0.810	575	20	0.42

FIGURE CAPTIONS

Fig. 1 Schematics of the SimVal combustor and the LSI

Fig. 2. Experimental conditions used for this study.

Figure 3. Visible luminosity of CH/H₂ LSI flames at 0.405 MPa, ϕ = 0.4 and U₀ = 40 m/s.

Figure 4. Comparison of the flashback criterion, C_{quench}, of LSI and the baseline SV-HSI for 60% - 100% H₂ fuels at 0.101 < P₀ < 0.810 MPa, 500 < T₀ < 600K and 0.4 < ϕ < 0.7

Figure 5. Mean velocity vectors for three H₂/CH₄ flames at STP, U₀ = 18 m/s, and ϕ = 0.4.

Figure 6. Centerline profiles of the STP LSI flames.

Figure 7. Virtual origin, x₀ (a), normalized axial divergence, a_x, (b) of the STP flames and their turbulent flame speeds (c).

Figure 8. Radial profiles (at x = 15 mm) of the STP LSI flames. Symbol legend same as in Fig. 6.

Figure 9. Mean flame brush positions of the NG/H₂.

Figure 10. NO_x emissions of the LSI compared with the baseline HSI configuration.

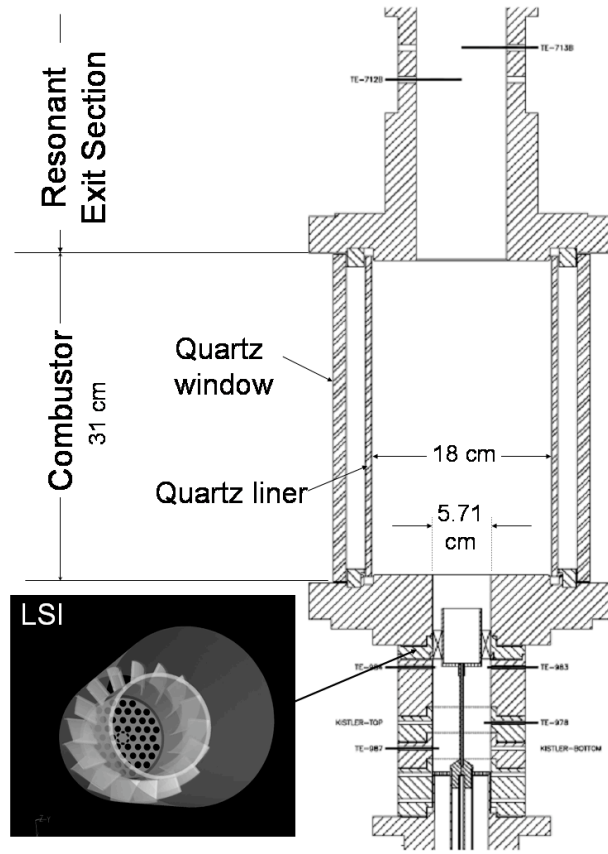


Figure 1 Schematics of SimVal and the low-swirl injector.

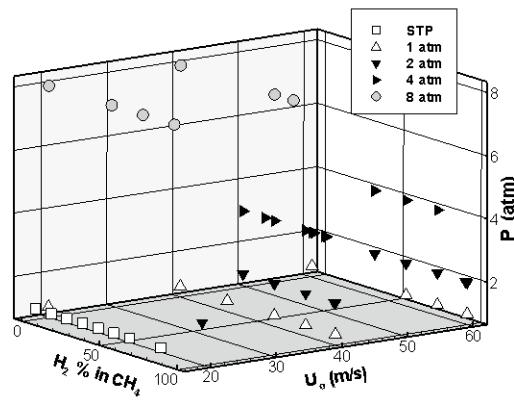


Figure 2 Experimental conditions for this study.

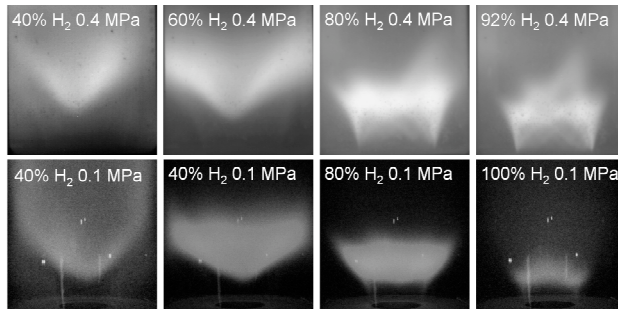


Figure 3 Visible luminosity of CH₄/H₂ LSI flames: top row 0.405 MPa, $\phi = 0.4$ and $U_0 = 40$ m/s and bottom row 0.101 MPa, $\phi = 0.4$ and $U_0 = 18$ m/s.

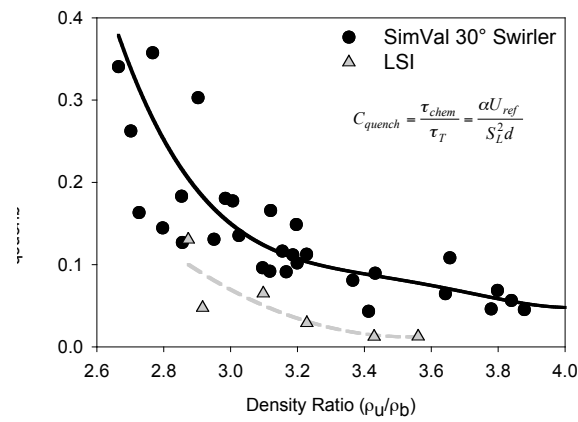


Figure 4 C_{quench} , of LSI and the baseline SV-HSI for 60% - 100% H₂ fuels at $0.101 < P_0 < 0.810$ MPa, $500 < T_0 < 600$ K and $0.4 < \phi < 0.7$.

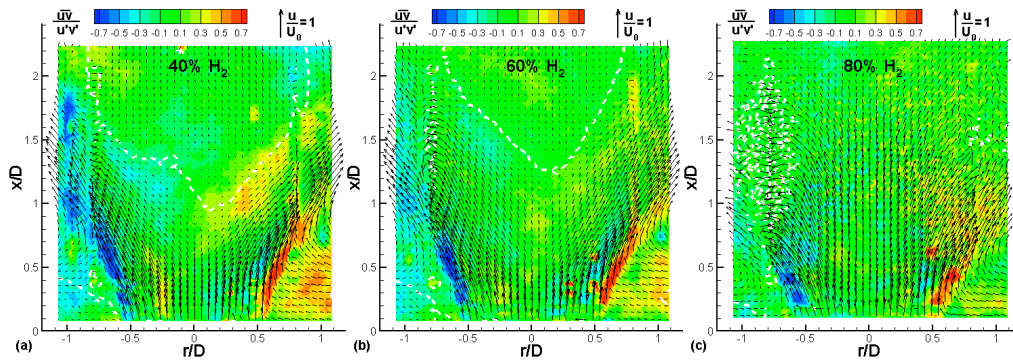


Figure 5 Mean velocity vectors for three H₂/CH₄ flames at STP, $U_0 = 18$ m/s, and $\phi = 0.4$. Color contours of the normalized shear stresses are show in the background.

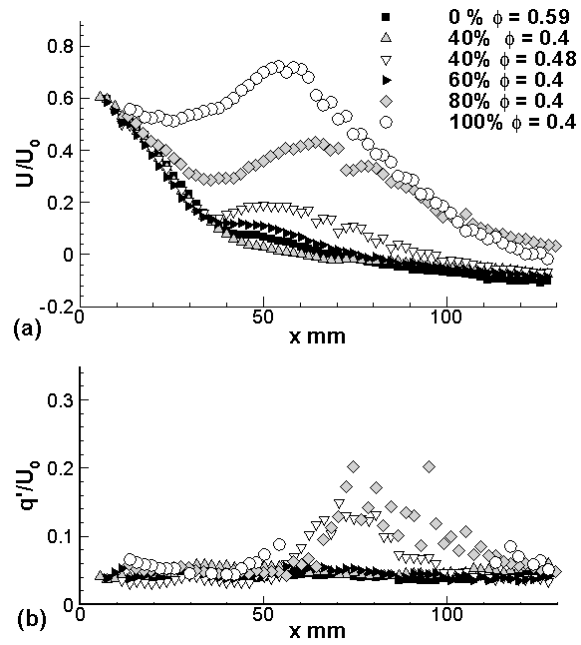


Figure 6 Centerline profiles of the STP LSI flames.

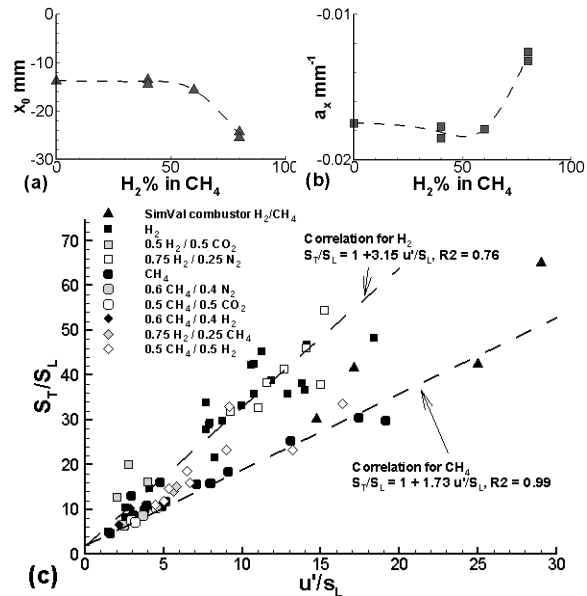


Figure 7 x_0 (a), a_x (b) of the STP flames and their S_T (c).

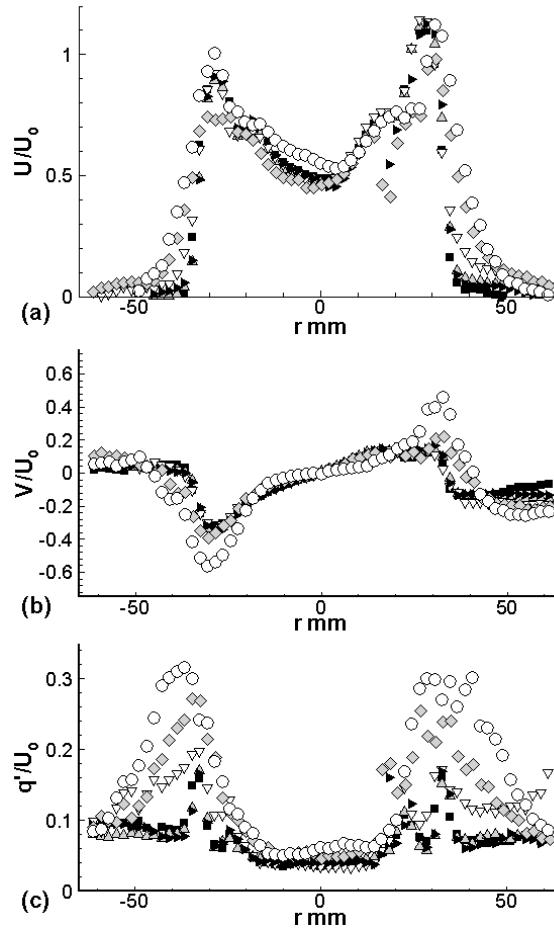


Figure 8 Radial profiles (at $x = 15$ mm) of the STP LSI flames. Symbol legend same as in Fig. 6.

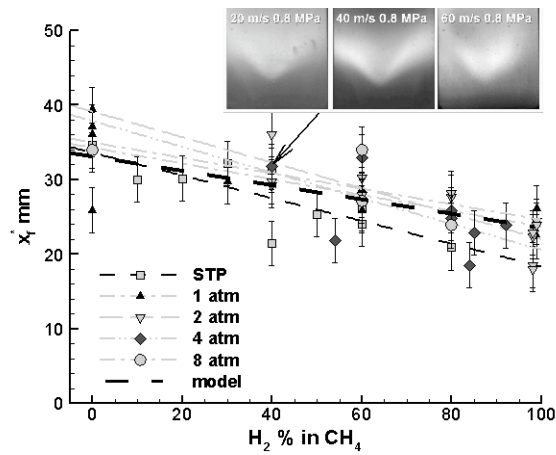


Figure 9 Mean flame brush positions of the NG/H₂ flames

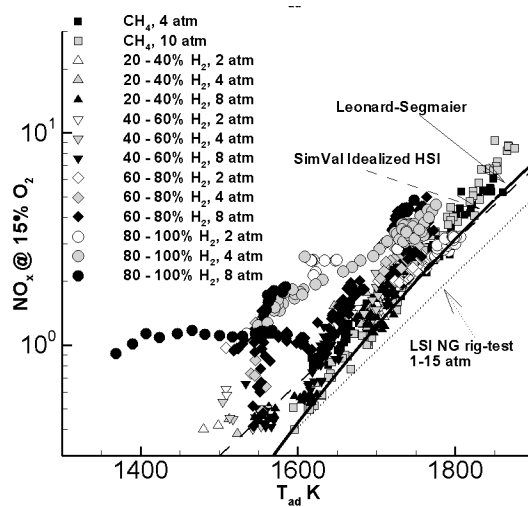


Figure 10 NO_x emissions of the LSI compare with the baseline HSI configuration.